Biomaterials Science

PAPER

View Article Online
View Journal | View Issue

Cite this: *Biomater. Sci.*, 2018, **6**, 136

Variation of the bone forming ability with the physicochemical properties of calcium phosphate bone substitutes

Rongquan Duan,[a,b,c] Davide Barbieri,[b] Xiaoman Luo,[b] Jie Weng,[c] Chongyun Bao,[d] Joost D. de Bruijn[a,b,e] and Huipin Yuan*[b,f,g]

Because of their bioactive properties and chemical similarity to the inorganic component of bone, calcium phosphate (CaP) materials are widely used for bone regeneration. Six commercially available CaP bone substitutes (Bio-Oss, Actifuse, Bi-Ostetic, MBCP, Vitoss and chronOs) as well as two tricalcium phosphate (TCP) ceramics with either a micron-scale (TCP-B) or submicron-scale (TCP-S) surface structure are characterized and their bone forming potential is evaluated in a canine ectopic implantation model. After 12 weeks of implantation in the paraspinal muscle of four beagles, sporadic bone (0.1 ± 0.1%) is observed in two Actifuse implants (2/4), limited bone (2.1 ± 1.4%) in four MBCP implants (4/4) and abundant bone (21.6 ± 4.5%) is formed in all TCP-S implants (4/4). Bone is not observed in any of the Bio-Oss, Bi-Ostetic, Vitoss, chronOs and TCP-B implants (0/4). When correlating the bone forming potential with the physicochemical properties of each material, we observe that the physical characteristics (*e.g.* grain size and micropore size at the submicron scale) might be the dominant trigger of material directed bone formation *via* specific mechanotransduction, instead of protein adsorption, surface mineralization and calcium ion release.

Received 7th August 2017,
Accepted 19th October 2017

DOI: 10.1039/c7bm00717e

rsc.li/biomaterials-science

1. Introduction

Calcium phosphate (CaP) ceramics, such as beta-tricalcium phosphate (β-TCP), hydroxyapatite (HA) and biphasic calcium phosphate (BCP), have been developed to aid the healing of bone defects.[1,2] Next to their biocompatibility, bioactivity and osteoconductivity, CaP ceramics with specific physicochemical properties have also been shown to initiate bone formation on their surface after ectopic implantation (*e.g.* intramuscular, and subcutaneous). As bone cells are not present at these locations, this phenomenon is described as material directed bone formation (*i.e.* osteoinduction).[3–5]

With the ability to induce bone formation, osteoinductive CaP bone substitutes do not only trigger bone formation faster than those lacking osteoinductivity,[6] but also allow the repair of critical-sized bone defects.[7,8] Moreover, an osteoinductive CaP bone substitute showed an equal bone regeneration capacity to autograft and collagen load with recombinant human bone morphogenetic protein 2 (rhBMP-2) in critical bone defects.[9] The osteoinductive potential of CaP materials is largely dependent on their physicochemical properties.[10–18] The chemical composition plays a role in inductive bone formation. For instance, BCP (*i.e.* biphasic ceramic of HA and TCP) has a higher osteoinductive potential than HA,[6,10] indicating a role of the faster resorbing TCP. However, a negative influence of the TCP content was reported in a study where an increase of TCP in CaPs adversely affected the osteoinductive ability and no bone formation was detected in pure TCP ceramics.[11] Next to the chemistry, the presence of micropores in the material has proven to be crucial for osteoinduction.[12] For example, Ariizumi *et al.* found that TCP with interconnected macropores and micropores gave rise to inductive bone formation while in the absence of micropores it did not.[13] Furthermore, it was shown that the osteoinductive potential increased with microporosity.[14] Moreover, the size of micropores has also been reported to greatly affect inductive bone formation by CaP ceramics. For instance, a study where two BCP ceramics were compared in the muscle of goats showed

[a]*Biomaterials Science and Technology, MIRA Institute, University of Twente, 7500 AE, Enschede, the Netherlands*
[b]*Kuros Biosciences BV, 3723 MB, Bilthoven, the Netherlands*
[c]*Key Laboratory of Advanced Technologies of Materials, Ministry of Education, School of Materials Science and Engineering, Southwest Jiaotong University, Chengdu 610031, China*
[d]*State Key Laboratory of Oral Diseases, West China School of Stomatology, Sichuan University, Chengdu 610041, China*
[e]*School of Engineering and Materials Science, Queen Marry University of London, E14RD, London, UK*
[f]*Complex Tissue Regeneration department, MERLN Institute for Technology Inspired Regenerative Medicine, Maastricht University, 6229 ER, Maastricht, the Netherlands. E-mail: h.yuan@maastrichtuniversity.nl; Fax: +31-30-2297299; Tel: +31-30-2297292*
[g]*College of Physical Science and Technology, Sichuan University, Chengdu, China*

that only the BCP with a smaller pore size and crystal size induced bone formation.[15]

Given the fact that osteoinduction of CaP materials is material-dependent, it is likely that the bone forming potential of commercially available CaP bone substitutes varies due to differences in their physicochemical properties. In this study, six commercially available CaP bone substitutes (Bio-Oss, Actifuse, Bi-Ostetic, MBCP, Vitoss and chronOs) as well as two β-TCP ceramics with either a micron-scale (TCP-B) or submicron-scale (TCP-S) surface architecture were characterized and their intramuscular bone forming potential was evaluated using a well-established canine osteoinduction study model.[8,16]

2. Experimental section

2.1. Calcium phosphate materials and characterization

2.1.1. Calcium phosphate materials. Six CaP bone substitutes (Bio-Oss, Actifuse, Bi-Ostetic, MBCP, Vitoss and chronOs) (Table 1) were purchased and used as received. Two β-TCP ceramics with micron (TCP-B) or submicron (TCP-S) granules were prepared as previously described[8] and were sterilized with gamma irradiation (dose 25–40 kGy, Isotron Netherland BV, Ede, the Netherlands) prior to use.

2.1.2. Physicochemical characterization. The chemistry and crystal structure of the eight CaP materials were evaluated with X-ray diffraction (XRD, Miniflex II, Rigaku, Tokyo, Japan). The surface structure of the materials was observed with a scanning electron microscope (SEM, JEOL JSM-5600, JEOL Ltd, Tokyo, Japan). The grain size (the vertical lengths crossing the center of each grain) was measured by randomly selecting 100 grains from 10 SEM images (×5000). The microporosity (*i.e.* the volume percentage of pores smaller than 10 μm in the material), micropore size distribution, and surface area were obtained by mercury intrusion (n = 1 per material, Micromeritics Instrument Incorporation, Norcross, USA).

2.1.3. Protein adsorption. The materials (0.1 cc ml^{-1}, triplicates) were immersed in cell culture medium [minimal essential medium-alpha (α-MEM, Gibco, Invitrogen, UK) supplemented with 10% fetal bovine serum (FBS, Lonza, Germany) and 1% penicillin/streptomycin (Gibco, Invitrogen, UK)], and incubated at 37 °C under a humid atmosphere with 5% CO_2 for 4 days. After washing three times with phosphate buffer solution (PBS, Invitrogen, Darmstadt, Germany), 0.5 ml of 1% Triton solution was added to each sample. Thereafter, the amount of protein detached from the samples into the Triton solution was measured with the QuantiPro™ BCA Assay Kit (Pierce Biotechnology Inc., Rockford, USA) following the manufacturer's instructions and the absorbance was measured with a spectrophotometer (Anthos Zenyth 3100, Anthos Labtec Instruments GmbH, Salzburg, Austria) at 620 nm. Protein adsorption was converted to the same amount of the material used for the *in vivo* implants (1.0 cc) and expressed as mean ± SD.

2.1.4. Release of calcium and phosphate ions. With stirring at 70 rpm and at 37 °C, 0.5 cc of each material (in triplicate) was incubated in a 100 ml simulated physiological saline solution (SPS, 0.8% NaCl, 50 mM HEPES, 0.4 mM NaN_3, 37 °C, pH = 7.3) for 1, 4 and 7 days. Calcium and phosphate concentrations in the SPS solution were measured with a QuantiChrom™ Calcium assay kit (BioAssay Systems, Hayward, USA) and PhosphoWorks™ Colorimetric Phosphate assay kit (AAT Bioquest®, Inc., Sunnyvale, USA) respectively following the manufacturer's guidelines. Thereafter, the absorbance was measured with a spectrophotometer (Anthos Zenyth 3100, Anthos Labtec Instruments GmbH, Salzburg, Austria) at 620 nm. The calcium and phosphate concentrations were quantified respectively with a standard calibration curve and expressed as mean ± SD.

2.1.5. Surface mineralization. The bioactivity of the materials was evaluated *in vitro* with a simulated body fluid (SBF).[17] SBF was prepared by dissolving reagent grade chemicals in distilled water (1000 ml) strictly in the order of NaCl (8.035 g), $NaHCO_3$ (0.355 g), KCl (0.225 g), $K_2HPO_4 \cdot 3H_2O$ (0.231 g), $MgCl_2 \cdot 6H_2O$ (0.311 g), $CaCl_2$ (25 ml) (calcium ion standard solution, 0.1 M, Metrohm, Herisau, Switzerland) and Na_2SO_4 (0.072 g). The solution was then buffered to pH = 7.4 at 36.5 °C with Tris $(CH_2OH)_3CNH_3$ (6.118 g) and 1 M HCl (25 ml). Fifty granules of each material as well as aluminum

Table 1 Physicochemical properties of calcium phosphate materials

Material	Supplier	Chemistry[a]	Micropore size[b]	Grain size[c] [μm]	Surface structure dimension	Micro porosity[b] [%]	Specific surface area by weight[b] [m^2 g^{-1}]	Specific surface area by volume[b] [m^2 ml^{-1}]
Bio-Oss	Geistlich Pharma AG	HA	Nano	Nano-scale	Nano	43.01	28.46	18.01
Actifuse	Apatech Baxter	Si-HA	Micron	1.02 ± 0.43	Micron	22.05	0.33	0.32
MBCP	Biomatlante	55HA/45TCP	Submicron	0.71 ± 0.20	Submicron	40.53	2.93	2.09
Bi-Ostetic	Berkeley Advanced Biomaterials	45HA/55TCP	Micron	0.91 ± 0.24	Micron	53.74	1.42	1.10
Vitoss	Orthovita Stryker	TCP	Micron	1.93 ± 0.70	Micron	42.74	0.36	0.30
ChronOs	Synthes	TCP	Micron	5.03 ± 1.90	Micron	31.52	0.51	0.59
TCP-B	Home made	TCP	Micron	2.52 ± 0.34	Micron	46.32	0.83	0.73
TCP-S	Home made	TCP	Submicron	0.81 ± 0.21	Submicron	45.14	1.85	1.59

[a] As evaluated by X-ray diffractometry. [b] Obtained from mercury intrusion. [c] As confirmed by quantitative measurements from scanning microscopy images (5000×).

oxide ceramic granules (an internal negative control[18] and prepared as described elsewhere[19]) were soaked in 200 mL of SBF at 37 °C for up to 14 days. A minimum of 5 granules were taken out at each time point of 1, 4, 7, and 14 days. The granules collected were carefully rinsed with distilled water, dried, gold-sputtered and observed with SEM in the secondary electron modality.

2.2. Ectopic bone formation

2.2.1. Animal experiments. All animal experiments were performed in compliance with the laws and institutional guidelines of the local animal care committee. After approval of the local animal care committee (*i.e.* the management committee of experimental animals of Sichuan province, China), the eight CaP materials (n = 4, 1.0 cc per material) were intramuscularly implanted in the paraspinal muscles of 4 canines (beagles, male, 12 month old, 8 samples per animal). The surgical operation was conducted under general anesthesia by intravenous injection of sodium pentobarbital (30 mg per kg body weight) and sterile conditions. Following the surgeries, buprenorphine (0.1 mg per animal) was intramuscularly injected into the dogs for 2 days to relieve pain, while penicillin (40 mg kg^{-1}) was intramuscularly injected for three consecutive days to prevent infection. After operation, the animals received a normal diet. Fluorochromes were intravenously injected at 3 weeks (calcein, Sigma, Louis, USA, 10 mg kg^{-1}), 6 weeks (xylenol orange, Sigma, 50 mg kg^{-1}) and 9 weeks (tetracycline, Sigma, 10 mg kg^{-1}) after surgery to monitor the onset time of bone formation. Twelve weeks after operation, the animals were sacrificed by a celiac injection of an excessive amount of pentobarbital sodium, and implants were harvested with the surrounding tissues.

2.2.2. Histological and histomorphometric analysis. The explants were fixed in 4% buffered formaldehyde solution (pH = 7.4) at 4 °C for one week, then dehydrated with a series of gradient ethanol solutions and finally embedded in methyl methacrylate (MMA, K-plast, LTI Netherland, Bilthoven, the Netherlands). Serial non-decalcified sections with an average thickness of 10–20 μm were obtained using a microtome (SP-1600, Leica, Wetzlar, Germany) equipped with a diamond saw blade. Sections for light microscopy observation were stained with 1% methylene blue (Sigma-Aldrich, Louis, USA) and 0.3% basic function (Sigma-Aldrich) after etching with acidic ethanol (Merck, Darmstadt, Germany). Non-stained sections were used for fluorescence microscopic observation with the FITC Texas Red filter (bandpass mirror wavelengths of 510–555 nm and 585–665 nm; Nikon, Tokyo, Japan). Overview images were obtained from the stained sections with a slide scanner (Dimage Scan Elite 5400II, Konica Minolta Photo Imaging Inc., Tokyo, Japan) for histomorphometric analysis, which was performed using Adobe Photoshop Elements 4.0 software (CS5, v12, Adobe Systems Benelux BV, Amsterdam-Zuidoost, the Netherlands). The area with CaP materials was selected as a region of interest (ROI) and the corresponding number of pixels was read as ROI. Then the bone tissue area and CaP materials were pseudo-colored and their respective pixels were counted as B and M respectively. The percentage of bone in the available space was determined as $B\% = B \times 100/(\text{ROI} - M)$ and presented as mean ± SD.

2.3. Statistics

Statistical analysis was carried out using one-way analysis of variance (ANOVA) with Tukey's test. Differences were considered statistically significant at $p < 0.05$.

3. Results

3.1. Calcium phosphate materials and characterization

3.1.1. Physicochemical properties of the CaP materials. The physicochemical properties of the materials are summarized in Table 1. The XRD patterns (Fig. 1) show that the CaP materials are chemically different and consist of HA (Bio-Oss and Actifuse) or TCP (Vitoss, chronOs, TCP-B and TCP-S) or BCP (Bi-Ostetic and MBCP). The wider peaks in the XRD pattern of Bio-Oss indicate its less crystalline nature compared to the other materials. The SEM images show that the eight CaP materials have different surface structures regarding the grain size, the dimensions and the amount of micropores (Fig. 2 and Table 1). Mercury intrusion data indicate variations in the micropore size, micropore distribution, microporosity and specific surface area among these CaP materials (Table 1 and Fig. 2A). The nano-scaled crystal grains and nano-scaled micropores indicate that Bio-Oss has a nano-scale surface architecture. Having both the crystal grains and the micropores smaller than 1 μm, MBCP and TCP-S belong to submicron-scale surface structured CaP materials. With either crystal grains or micropores larger than 1 μm, the surface structure of Actifuse, Bi-Ostetic, Vitoss, chronOs and TCP-B is at the micron scale.

3.1.2. Release of calcium and phosphate ions. The release of calcium and phosphate ions from the CaP materials into the SPS solution varied with the content of TCP components. In general, TCP materials (Vitoss, TCP-S, TCP-B and chronOs)

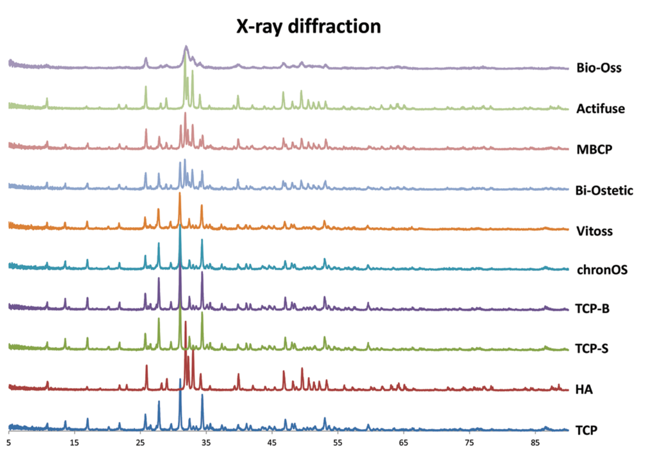

Fig. 1 XRD pattern showing the chemistry of the eight CaP materials compared with standard HA and β-TCP.

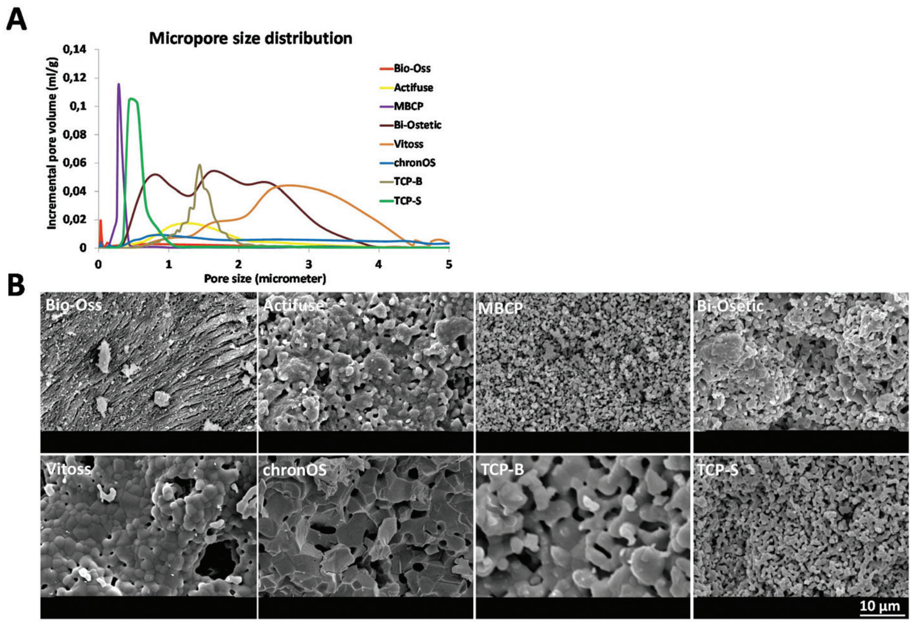

Fig. 2 A: Distribution plots of the micropore with size; B: SEM images showing the surface structure of seven CaP materials.

released the most calcium and phosphate ions, while HA materials (Bio-Oss and Actifuse) released the least, with the BCP materials (Bi-Ostetic and MBCP) in between (Fig. 3B and C). In addition, having the same chemistry, Vitoss released more calcium and phosphate ions, followed by TCP-S, TCP-B and chronOs.

3.1.3. Protein adsorption. The amount of protein adsorbed by the eight CaP materials is shown in Fig. 3A, and it is related to the specific surface area of the materials. Having the largest surface area (18.01 m^2 ml^{-1}), Bio-Oss has the highest protein adsorption capacity, followed by MBCP, TCP-S, Bi-Ostetic, TCP-B and chronOs. Because of their smaller surface area, Vitoss (0.30 m^2 ml^{-1}) and Actifuse (0.32 m^2 ml^{-1}) adsorbed the least.

3.1.4. Surface mineralization. No apatite was formed on the surface of alumina ceramics after 14 days of soaking in SBF (data not shown), which validated the *in vitro* bioactivity evaluation system.[17,18] The layers of CaP apatite were formed on the surface of all the tested materials after 1 day soaking in SBF at 37 °C (Fig. 3D), but the degree of mineralization varied among the CaP materials. Scattered mineralization was detected on the surface of Vitoss, chronOs and TCP-B, while the rest of the other materials were completely covered by a layer of mineralized apatite. With the soaking time, the apatite layers gradually deposited eventually covering the surface of all CaPs after 14 days of soaking in SBF.

3.2. Tissue response after intramuscular implantation of the CaP materials

The newly formed bone was observed in TCP-S (4 out of 4), MBCP (4 out of 4) and Actifuse implants (2 out of 4), while no bone formation was seen in any of Bio-Oss, Bi-Ostetic, Vitoss, chronOs and TCP-B (Fig. 4).

Normal bone structures with osteocytes embedded in the lacunae and osteoblasts laid on *de novo* bone were often observed in TCP-S and MBCP implants, while sporadically in Actifuse implants (Fig. 5). In addition, macrophage-like cells engulfing fine ceramic particles were mainly observed in TCP-S and MBCP samples (Fig. 5).

Under fluorescence microscopy, three colors (green, calcein, 3 weeks; red, xylenol orange, 6 weeks; and yellow, tetracycline, 9 weeks) were seen in TCP-S implants, while only green color was observed in MBCP, Actifuse, Bio-Oss and Bi-Ostetic implants, and no color was detected in Vitoss, chronOs and TCP-B implants (Fig. 6). Since the green color was seen in the CaP materials, it suggests mineralization *in vivo*. The red and yellow colors stained the bone tissues in TCP-S implants, indicating that the bone formation started between 3 and 6 weeks after implantation, and bone was still actively formed at week 9. Red and yellow colors were not seen in MBCP and Actifuse implants, suggesting that the bone formation process in these two materials started 9 weeks after implantation.

Quantitatively TCP-S gave rise to significantly more bone formation in the available space (21.6 ± 4.5%) than MBCP (2.1 ± 1.4%). The bone formed in Actifuse (0.1 ± 0.1%) was significantly less than that in TCP-S and MBCP (Fig. 7).

4. Discussion

4.1. Which material factors are triggers for ectopic bone formation?

In the current study, Actifuse, MBCP and TCP-S implants triggered bone formation after 12 weeks, with different incidences, onset times and amounts of bone. No bone formation was detected in Bio-Oss, Bi-Ostetic, Vitoss, chronOs

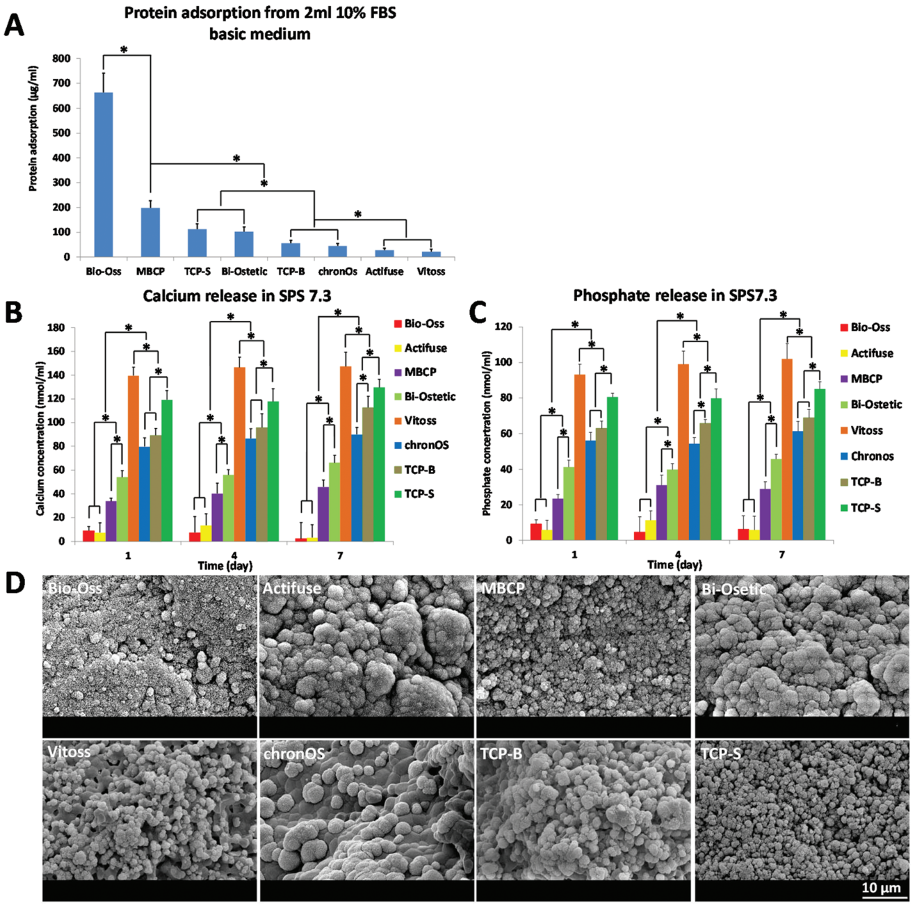

Fig. 3 A: Amount of proteins adsorbed onto implants (1 ml) from culture medium after 4-day incubation; B, C: release of calcium and phosphate ions from the materials into SPS at day 1, day 4 and day 7 (*$p < 0.05$); D: SEM images showing the apatite formation on the seven CaP materials after soaking in SBF for 1 day.

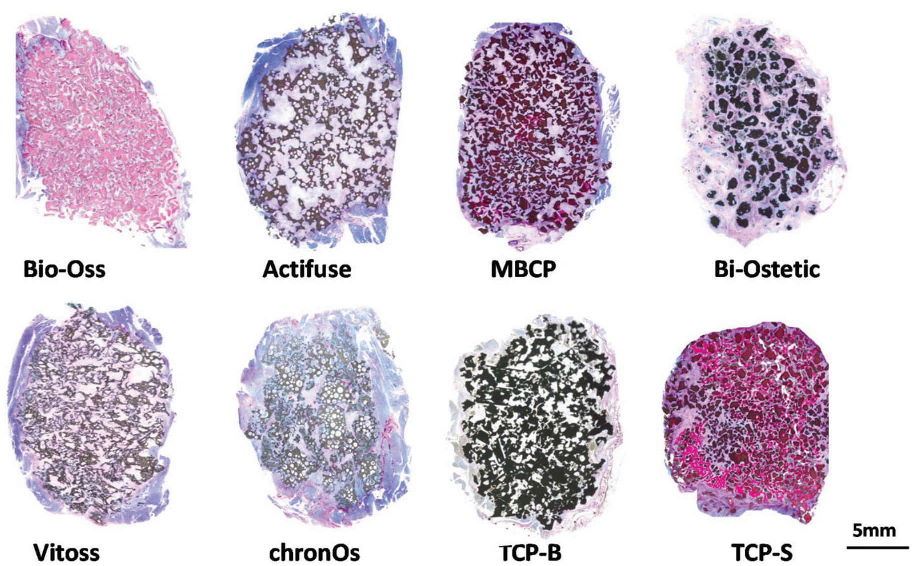

Fig. 4 The histological overviews showing the tissue formation in CaP materials intramuscularly implanted in beagles for 12 weeks (un-decalcified sections stained with methylene blue and basic fuchsin, bone was stained fresh-red).

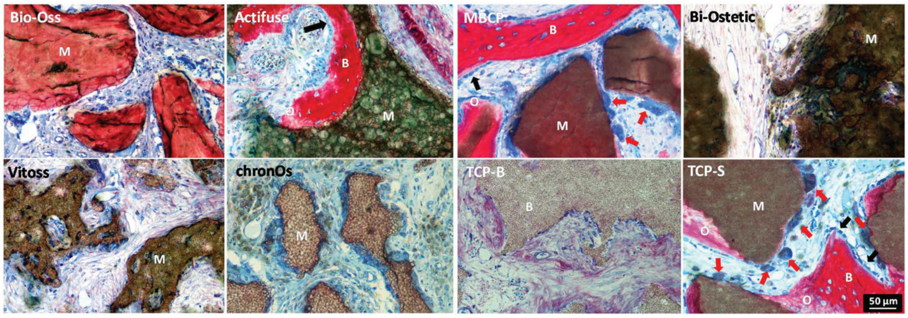

Fig. 5 Histological images showing tissue responses to CaP materials intramuscularly implanted in beagles for 12 weeks (B: bone; M: material; O: osteoid; black arrow: osteoblast, red arrow: foreign body giant cells).

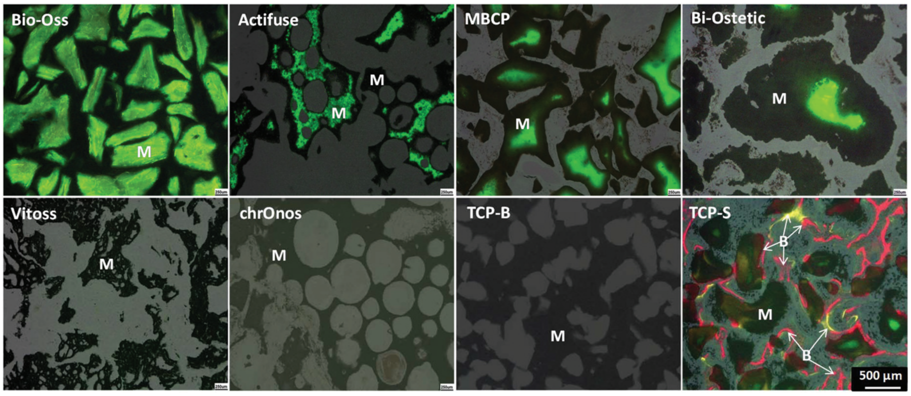

Fig. 6 The fluorescence images showing the mineralization of materials and the onset time of bone formation within CaP materials intramuscularly implanted in beagles for 12 weeks (green, calcein, 3 weeks; red, xylenol orange, 6 weeks; yellow, tetracycline, 9 weeks; M: materials; B: bone).

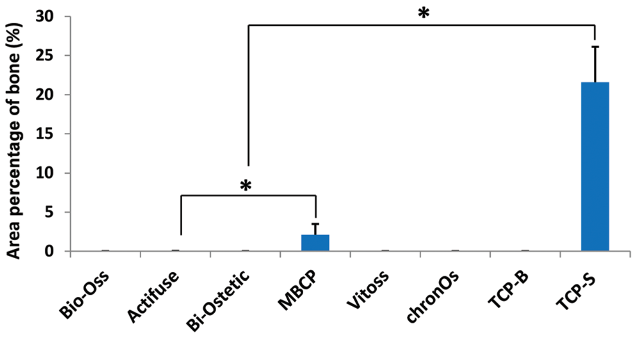

Fig. 7 The area percentage of bone in the available spaces of the CaP material implants (*$p < 0.05$).

and TCP-B. The ectopic bone forming potential among the eight CaP materials is related to their physicochemical properties.

4.1.1. Chemical composition. When the chemical composition was evaluated as a potential material factor for inductive bone formation, the influence of the HA/TCP ratio was observed in individual studies.[6,10,11] In this study, bone formation was induced in Actifuse (Si-HA), MBCP (BCP) and TCP-S (TCP), indicating that osteoinduction was not constrained to only one chemistry. It has been reported that the presence of TCP could release more calcium and phosphate thus enhancing inductive bone formation.[6,10] However, despite their identical chemistry, we observed that Vitoss released most calcium and phosphate ions *in vitro* but did not induce any bone formation while TCP-S did. Similarly, Bio-Ostetic contained more TCP and released more calcium and phosphate ions than MBCP, but it was MBCP rather than Bio-Ostetic to induce bone formation. Furthermore, other studies demonstrated that some materials free of CaP induced ectopic bone formation.[19,20] Therefore, the chemical composition may not be appointed as a determinant trigger in CaP material-driven osteoinduction.

4.1.2. Macroporous structure. Bone formation has never been observed in the dense structure of CaPs and was always detected in the pores of osteoinductive CaPs, indicating the necessity of macroporous structures in inductive bone formation.[3–6] All eight CaP materials evaluated in this study have macroporous structures, but only three of them induced ectopic bone formation, suggesting that the macrostructural property is a prerequisite but is not a sufficient factor to trigger osteoinduction.

4.1.3. Microporous structure. Micropores (*i.e.* smaller than 10 µm) and microporosity have been shown to be essential for

CaP material-driven osteoinduction.[12–15] In the current study, when TCP-S was compared to chronOs, the role of microporosity in inductive bone formation was shown. The higher microporosity in TCP-S led to inductive bone formation, while the less microporous chronOs did not. However, given the same chemistry and similar microporosity, TCP-S induced bone while TCP-B and Vitoss did not. This indicates that the high microporosity does not guarantee inductive bone formation in CaP materials. At the same time, the variation in the micropore size and crystal grain size among TCP-S, TCP-B and Vitoss suggests the importance of the dimension of the surface structure in material-driven osteoinduction, which was further confirmed in BCP materials. In fact, despite having higher microporosity than MBCP, Bi-Ostetic did not induce bone formation but MBCP with a finer pore and grain size did. It should be stressed again that MBCP and TCP-S have different chemistries but a similar submicron scale structure, and both induced bone formation. Furthermore, having either a nano-scale (Bio-Oss) or micron-scale (Vitoss, Bi-Ostetic, chronOs and TCP-B) surface structure, the materials did not induce any bone formation. These results suggest the essential role of the surface structure when at the submicron scale rather than at the nano- or micron-scale as a trigger in CaP material-driven bone formation. Despite its micron-scale surface architecture, Actifuse triggered sporadic bone formation which may be attributed to silicon incorporation.[21]

We have previously said that the chemistry may not be a crucial trigger of material-driven bone formation. However, once the bone formation process is triggered, TCP-S having more TCP content induced more bone compared with MBCP. Therefore, the influence of the chemistry on inductive bone formation is still important for the quantity of new bone tissue formation.

4.2. How do material factors trigger bone formation?

As described above, the surface structure at the submicron-scale may be the essential trigger for osteoinduction by CaP materials, but how it triggers CaP-induced bone formation is not clear as yet. It is generally thought that bone induction of CaP materials is the result of protein adsorption,[3,5,9,13,22,23] surface mineralization[10,24,25] and calcium and phosphate ions release.[26–28]

4.2.1 Protein adsorption. When CaP materials are implanted in the body, they adsorb proteins from the body fluids (including growth factors). Inductive bone formation of CaP materials was often addressed as the secondary response of protein adsorption.[22,23] Indeed the protein adsorption theory explains well the role of the presence of micropores (including the quantity of micropores) and the size of the crystal grains and micropores in CaP-induced bone formation.[3,5,9,13] In the presence of micropores and with the decrease in the size of micropores and crystal grains, the specific surface area of CaP materials increases and more proteins can be concentrated favoring bone induction. However, the protein adsorption theory is not fully demonstrated because the possible proteins involved in material-induced bone formation were not identified. The data obtained in the current study do not support the protein adsorption theory either. When the same volume of CaP materials was soaked in simulated body fluids (cell culture medium containing foetal bovine serum), a large amount of proteins was adsorbed onto Bio-Oss, which has the highest surface area but no bone was formed in any of Bio-Oss implants.

4.2.2. Surface mineralization. Next to the protein adsorption, the ability to favor mineral deposition from body fluids appears to be a characteristic of osteoinductive materials as it could facilitate osteogenesis and explained bone induction in surface-active titanium implants.[29] The surface area and chemical composition of CaP materials affect the dissolution and reprecipitation events eventually leading to the formation of an apatite layer on their surface.[10,24] However, as seen in the current study, the green signal of calcein was present in Bio-Oss, Actifuse, Bi-Ostetic, MBCP and TCP-S implants but not in Vitoss, chronOs and TCP-B (Fig. 6). As fluorochromes form chelate complexes with apatite *via* their iminodiacetic acid groups, which is a phenomenon depending on the availability of the binding sites that could originate from the ongoing bone formation or surface mineralization processes.[30,31] Thus, the green color observed in implants indicates *in vivo* biomineralization of materials within 3 weeks after implantation. Cerruti *et al.*[32] also showed that the higher surface area led to faster compositional changes in the surrounding fluids hence facilitating early apatite formation. Bio-Oss, with the highest surface area and more amorphous structure, had the strongest calcein signal. Because of their lower surface area, Vitoss, chronOs and TCP-B did not mineralize *in vivo* and thus no calcein was detected in the implants. The *in vivo* mineralization is well correlated with the 1-day *in vitro* data, where scattered mineralization was observed on the surface of Vitoss, chronOs and TCP-B, while all the other materials were completely covered by a layer of mineralized apatite. Actifuse has a similar specific surface area to Vitoss, but the former underwent mineralization *in vivo* and was completely covered by an apatite layer *in vitro*, which might be attributed to the silica incorporation.[21] Nevertheless, mineralization occurred in all materials *in vitro*, and in 5 out of 7 materials *in vivo*, but only 3 of them induced bone formation. This suggests that surface mineralization of CaP materials may be a prerequisite but is not sufficient to trigger ectopic bone formation.

4.2.3. Release of calcium and phosphate ions. CaP materials could release calcium and phosphate ions with degradation or resorption. Such ions have shown their positive influence on the osteogenic differentiation of mesenchymal stem cells (MSCs) and the osteogenesis of osteogenic cells.[26–28] For instance, Shih *et al.* recently reported that phosphate ions released from CaP materials could induce osteogenic differentiation of human MSCs through phosphate-ATP-adenosine signaling.[28] It was thus assumed that bone induction by CaP materials could be the result of the release of calcium and phosphate ions. Indeed, the release of these ions may have enhanced the bone formation in CaP materials having a high content of TCP.[6,10,17] However, the release of calcium and phosphate ions may not be considered as the triggers of bone induction. As shown in Fig. 3B and C, Vitoss released the most calcium and phosphate ions but it did not induce bone formation at all. Furthermore, the ion release theory is not supported by the literature as other studies showed ectopic bone induction of non-CaP materials such as alumina[19] and polymeric implants.[20]

4.2.4. Surface topography. From the discussion above, the overall results in this study could not assign any of the biochemical theories of protein adsorption, surface mineralization and ion release to CaP-induced bone formation. Indeed, in the absence of chemical signals, special surface topographies, more especially with a scale range from nano- to micron-meters, have shown to directly modulate the cellular behavior and guide specific biological responses.[33–45] For example, Abagnale *et al.* found that ridges of 15 μm increased the differentiation of mesenchymal stem cells (MSCs) into adipogenic lineages, while smaller ridges enhanced osteogenic differentiation.[45] A similar phenomenon has been described by Hatano *et al.* who observed that the rough surface (0.81 μm) enhanced the proliferation, alkaline phosphatase (ALP) activity and osteocalcin expression of rat osteoblasts in comparison with the smoother one.[46] Presumably the submicron surface topography directly induces osteogenesis through mechanotransduction, *i.e.* the translation of mechanical stimuli at the cell–substrate interface into electrochemical signals which elicit specific cellar responses, through YAP and TAZ regulators.[47–49] It is also likely that through the mechanotransduction, mesenchymal stem cells adapt their shape to surface structure, recruit the TGF receptor on primary cilia and undergo osteogenic differentiation.[50]

In addition to modulating stem cells and osteoblasts, giant cells (*e.g.* macrophages) are sensitive to the surface topography. For instance, Fellah and colleagues observed that the amount of macrophages and giant cells varied according to the surface grain size of CaP ceramic implants.[51] Furthermore Davison *et al.* showed that CaP ceramics with submicron sized surface architecture could induce an inflammatory response of macrophages, and their subsequent secretion of cytokines induced stem cell differentiation.[16,52] In line with the findings by Kondo *et al.*, who observed plenty of active multinucleated giant cells prior to osteoinductive bone formation in CaP implants,[53] we observed in this study macrophage-like cells on the submicron structured surface of osteoinductive TCP-S and MBCP. It is possible that the crosstalk between macrophages and mesenchymal stem cells on the submicron scaled surface topography initiated the CaP-directed osteoinduction through mechanotransduction.

Osteoinductive CaP materials are useful for bone regeneration,[6–9] and identifying the crucial material factors would be helpful for further optimization of CaP materials with respect to the bone forming ability. The submicron dimension of the surface structure of CaP materials was clearly shown to be the stronger trigger of ectopic bone formation. However, more studies are necessary to further understand the material-driven osteoinduction from a biological perspective.

5. Conclusion

We compared the bone forming potential of eight synthetic CaP bone substitutes and found that the bone forming ability varied with materials. It was observed that the specific topography engineered by submicropores and submicron crystal grains appear to be the necessary trigger for osteoinduction, and that ceramics releasing ions could enhance the inductive bone formation. The submicron-scale surface topography, *via* specific mechanotransduction, might be the direct trigger of osteoinduction in CaP bone substitutes rather than the theories already in the literature such as protein adsorption, surface mineralization and calcium ion release.

Conflicts of interest

The authors declare no competing financial interest.

Acknowledgements

The authors would like to thank the Netherlands Institute for Regenerative Medicine (NIRM), Rapid Prototyping of Custom-Made Bone-Forming Tissue Engineering Constructs (RAPIDOS Project, Ref. NMP-2013-EU-China 604517), the Seventh Framework Programme of the European Union (REBORNE under grant agreement no. 241879) and the Horizon 2020 Framework Programme for the financial support to this research project (CHARME, grant agreement no. 674282).

References

1 S. Samavedi, A. R. Whittington and A. S. Goldstein, *Acta Biomater.*, 2013, **9**, 8037–8045.

2 B. Susmita and T. Solaiman, *Acta Biomater.*, 2013, **8**, 1401–1421.

3 H. Yamasaki, *Jpn. J. Oral Biol.*, 1990, **32**, 190–192.

4 X. Zhang, P. Zhou, J. Zhang, W. Chen and C. Wu, in *Bioceramics and the Human Body*, ed. A. Ravaglioli and A. Krajewski, Elsevier Applied Science, London and New York, 1991, pp. 408–415.

5 U. Ripamonti, *Clin. Orthop. Relat. Res.*, 1991, **269**, 284–294.

6 H. Yuan, C. A. van Blitterswijk, K. de Groot and J. D. de Bruijn, *J. Biomed. Mater. Res., Part A*, 2006, **78**, 139–147.

7 P. Habibovic, H. Yuan, M. van den Doel, T. M. Sees, C. A. van Blitterswijk and K. de Groot, *J. Orthop. Res.*, 2006, **24**, 867–876.

8 R. Duan, D. Barbieri, X. Luo, J. Weng, J. D. de Bruijn and H. Yuan, *J. Orthop. Res.*, 2016, **34**, 1865–1873.

9 H. Yuan, H. Fernandes, P. Habibovic, J. de Boer, A. M. Barradas, A. de Ruiter, W. R. Walsh, C. A. van Blitterswijk and J. D. de Bruijn, *Proc. Natl. Acad. Sci. U. S. A.*, 2010, **107**, 13614–13619.

10 P. Habibovic, H. Yuan, C. M. van der Valk, G. Meijer, C. A. van Blitterswijk and K. de Groot, *Biomaterials*, 2005, **26**, 3565–3575.
11 K. Kurashina, H. Kurita, Q. Wu and A. Ohtsuka, *Biomaterials*, 2002, **23**, 407–412.
12 B. H. Fellah, O. Gauthier, P. Weiss, D. Chappard and P. Layrolle, *Biomaterials*, 2008, **29**, 1177–1188.
13 T. Ariizumi, A. Ogose, N. Kondo, H. Kawashima, T. Hotta, N. Kudo, M. Hoshino, H. Inoue, H. Irie and N. Endo, *J. Biomater. Nanobiotechnol.*, 2013, **4**, 189–193.
14 O. Chan, M. J. Coathup, A. Nesbitt, C. Y. Ho, K. A. Hing, T. Buckland, C. Campion and G. W. Blunn, *Acta Biomater.*, 2012, **8**, 2788–2794.
15 P. Habibovic, T. M. Sees, M. A. van den Doel, C. A. van Blitterswijk and K. de Groot, *J. Biomed. Mater. Res., Part A*, 2006, **77**, 747–762.
16 N. L. Davison, X. Luo, T. Schoenmaker, V. Everts, H. Yuan, F. Barrère-de Groot and J. D. de Bruijn, *Eur. Cells Mater.*, 2014, **15**, 281–297.
17 T. Kokubo and H. Takadama, *Biomaterials*, 2006, **27**, 2907–2915.
18 H. Fischer, C. Niedhart, N. Kaltenborn, A. Prange, R. Marx, F. U. Niethard and R. Telle, *Biomaterials*, 2005, **26**, 6151–6157.
19 H. Yuan, J. D. de Bruijn, X. Zhang, C. A. van Blitterswijk and K. de Groot, presented in part at Eur. Conf. Biomater, Osteoinduction by porous alumina ceramic, London, UK, 09, 2001.
20 G. D. Winter and B. J. Simpson, *Nature*, 1969, **223**, 88–90.
21 L. C. Gerhardt and A. R. Boccaccini, *Materials*, 2010, **3**, 3867–3910.
22 T. Boix, J. Gómez-Morales, J. Torrent-Burgués, A. Monfort, P. Puigdomènech and R. Rodríguez-Clemente, *J. Inorg. Biochem.*, 2005, **99**, 1043–1050.
23 T. J. Webster, L. S. Schadler, R. W. Siegel and R. Bizios, *Tissue Eng.*, 2001, **7**, 291–301.
24 R. Z. LeGeros, *Chem. Rev.*, 2008, **108**, 4742–4753.
25 S. Fujibayashi, M. Neo, H. M. Kim, T. Kokubo and T. Nakamura, *Biomaterials*, 2004, **25**, 443–450.
26 A. M. Barradas, H. A. Fernandes, N. Groen, Y. C. Chai, J. Schrooten, J. van de Peppel, J. P. van Leeuwen, C. A. van Blitterswijk and J. de Boer, *Biomaterials*, 2012, **33**, 3205–3215.
27 S. Nakamura, T. Matsumoto, J. Sasaki, H. Egusa, K. Y. Lee, T. Nakano, T. Sohmura and A. Nakahira, *Tissue Eng., Part A*, 2010, **16**, 2467–2473.
28 Y. R. Shih, Y. Hwang, A. Phadke, H. Kang, N. S. Hwang, E. J. Caro, S. Nguyen, M. Siu, E. A. Theodorakis, N. C. Gianneschi, K. S. Vecchio, S. Chien, O. K. Lee and S. Varghese, *Proc. Natl. Acad. Sci. U. S. A.*, 2014, **111**, 990–995.
29 M. Takemoto, S. Fujibayashi, M. Neo, J. Suzuki, T. Matsushita, T. Kokubo and T. Nakamura, *Biomaterials*, 2006, **27**, 2682–2691.
30 T. C. Lee, S. Mohsin, D. Taylor, R. Parkesh, T. Gunnlaugsson, F. J. O'Brien, M. Giehl and W. Gowin, *J. Anat.*, 2003, **203**, 161–172.
31 S. M. van Gaalen, M. C. Kruyt, R. E. Geuze, J. D. de Bruijn, J. Alblas and W. J. Dhert, *Tissue Eng., Part B*, 2010, **16**, 209–217.
32 M. Cerruti, *Philos. Trans. R. Soc., A*, 2012, **370**, 1281–1312.
33 S. Mitragotr and J. Lahann, *Nat. Mater.*, 2009, **8**, 15–23.
34 J. Fu, Y. K. Wang, M. T. Yang, R. A. Desai, X. Yu, Z. Liu and C. S. Chen, *Nat. Methods*, 2010, **7**, 733–736.
35 H. J. Jeon, C. G. Simon and G. H. Kim, *J. Biomed. Mater. Res., Part B*, 2014, **102**, 1580–1594.
36 T. Steinberg, S. Schulz, J. P. Spatz, N. Grabe, E. Mussig, A. Kohl, G. Komposch and P. Tomakidi, *Nano Lett.*, 2007, **7**, 287–294.
37 K. R. Milner and C. A. Siedlecki, *J. Biomed. Mater. Res., Part A*, 2007, **82**, 80–91.
38 A. Verma, O. Uzun, Y. Hu, Y. Hu, H. S. Han, N. Watson, S. Chen, D. J. Irvine and F. Stellacci, *Nat. Mater.*, 2008, **7**, 588–595.
39 S. Oh, K. S. Brammer, Y. S. Li, D. Teng, A. J. Engler, S. Chien and S. Jin, *Proc. Natl. Acad. Sci. U. S. A.*, 2009, **106**, 130–135.
40 C. H. Choi, S. H. Hagvall, B. M. Wu, J. C. Y. Dunn, R. E. Beygui and C. J. Kim, *Biomaterials*, 2007, **28**, 1672–1679.
41 M. J. Dalby, N. Gadegaard, R. Tare, A. Andar, M. O. Riehle, P. Herzyk, C. D. Wilkinson and R. O. Oreffo, *Nat. Mater.*, 2007, **6**, 997–1003.
42 E. K. Yim, R. M. Reano, S. W. Pang, A. F. Yee, C. S. Chen and K. W. Leong, *Biomaterials*, 2005, **26**, 5405–5413.
43 J. Lovmand, J. Justesen, M. Foss, R. H. Lauridsen, M. Lovmand, C. Modin, F. Besenbacher, F. S. Pedersen and M. Duch, *Biomaterials*, 2009, **30**, 2015–2522.
44 K. Kolind, D. Kraft, T. Bøggild, M. Duch, J. Lovmand, F. S. Pedersen, D. A. Bindslev, C. E. Bünger, M. Foss and F. Besenbacher, *Acta Biomater.*, 2014, **10**, 641–650.
45 G. Abagnale, M. Steger, V. H. Nguyen, N. Hersch, A. Sechi, S. Joussen, B. Denecke, R. Merkel, B. Hoffmann, A. Dreser, U. Schnakenberg, A. Gillner and W. Wagner, *Biomaterials*, 2015, **61**, 316–326.
46 K. Hatano, H. Inoue, T. Kojo, T. Matsunaga, T. Tsujisawa, C. Uchiyama and Y. Uchida, *Bone*, 1999, **25**, 439–445.
47 S. Dupont, L. Morsut, M. Aragona, E. Enzo, S. Giulitti, M. Cordenonsi, F. Zanconato, J. Le Digabel, M. Forcato, S. Bicciato, N. Elvassore and S. Piccolo, *Nature*, 2011, **474**, 179–183.
48 F. Gattazzo, A. Urciuolo and P. Bonaldo, *Biochim. Biophys. Acta*, 2014, **1840**, 2506–2519.
49 L. E. McNamara, R. J. McMurray, M. J. Biggs, F. Kantawong, R. O. Oreffo and M. J. Dalby, *J. Tissue Eng.*, 2010, **18**, 120623.

50 J. Zhang, M. T. Dalbay, X. Luo, E. Vrij, D. Barbieri, L. Moroni, J. D. de Bruijn, C. A. van Blitterswijk, J. P. Chapple, M. M. Knight and H. Yuan, *Acta Biomater.*, 2017, **57**, 487–497.
51 B. H. Fellah, B. Delorme, J. Sohier, D. Magne, P. Hardouin and P. Layrolle, *J. Biomed. Mater. Res., Part A*, 2010, **93**, 1588–1595.
52 N. L. Davison, A. L. Gamblin, P. Layrolle, H. Yuan, J. D. de Bruijn and F. Barrère-de Groot, *Biomaterials*, 2014, **35**, 5088–5088.
53 N. Kondo, A. Ogose, K. Tokunaga, H. Umezu, K. Arai, N. Kudo, M. Hoshino, H. Inoue, H. Irie, K. Kuroda, H. Mera and N. Endo, *Biomaterials*, 2006, **27**, 4419–4419.